A theoretical study of chiral carboxylic acids. Structural and energetic aspects of crystalline and liquid states

Angelo Gavezzotti[†] *and Leonardo Lo Presti*[*†,≈,∅]

[†] Università degli Studi di Milano, Department of Chemistry, Via Golgi 19, 20133 Milano (Italy)

[≈] CNR-ISTM, Via Golgi 19, 20133 Milano (Italy)

[∅] Center for Materials Crystallography, Aarhus University, Langelandsgade 140, DK-8000, Aarhus, Denmark

We would like to dedicate this paper to our longtime, unforgotten friend Peggy, appending a definition, impeccable, such as might have been written by Kurt Mislow, but found instead in a masterwork of the greatest Italian writer of the XXth century. The novel deals with matters highly spiritual, and not down-to-earth chemical, but chemistry, as Peggy so often said waving (metaphorically) the Merck Index, is everywhere.

"Destrogiri, sinistrogiri: termini della chimica strutturale, della geometria e della cristallografia: e diconsi, in genere, di due strutture molecolari simmetriche, cioè metricamente uguali ma non sovrapponibili (vite destra e vite sinistra).

Carlo Emilio Gadda, *La cognizione del dolore*, 2nd edition, Einaudi, Torino 1963, p.197

Please cite this work as
A. Gavezzotti, L. Lo Presti, Crystal Growth & Design 2015, 5 (8), pp 3792–3803

ABSTRACT

Lattice energy calculations by semiempirical and quantum mechanical methods have been carried out on 17 crystals of phenoxypropionic acids (PPAs), including 5 pairs of racemic and homochiral partners. Racemic crystals always consist of centrosymmetric cyclic hydrogen-bonded dimers, while homochiral crystals invariably include chain ("catemer") motifs of O-H···O hydrogen bonds, except for one case having a pseudo-twofold axis dimer with two molecules in the asymmetric unit. Energy differences between homochiral and racemic crystals are small, without a consistent trend of higher stability of either state. Partitioned molecule-molecule energy calculations show that hydrogen bonds are competing with diffuse dispersive factors or local electrostatic interactions. Monte Carlo methods with empirical atom-atom potentials were also applied to simulate the structural and energetic equilibrium properties of some racemic and homochiral liquids. The latter are very nearly isoenergetic, apparently irrespective of molecular size, shape and chemical constitution, and do not display significant differences in internal structure with respect to type, number, or persistency of hydrogen-bonded pairs. However, major changes in molecular conformation are predicted for PPAs upon crystallization. Based on these results, the roles of thermodynamics and kinetics are discussed in the context of understanding spontaneous resolution.

1. INTRODUCTION

One of the continuing mysteries of the solidification of chiral organic compounds from racemic solutions or liquids is the predominant formation of racemic crystals: spontaneous resolution into a conglomerate of enantiomeric chiral crystals is (very) seldom observed. The factors that control crystallization are scarcely known in general, and the racemic-homochiral dilemma is an added difficulty. Thermodynamic and kinetic factors are involved, of which we have relatively little command. Systematic analyses of homochiral and racemic crystal pairs have been carried out,[1,2] finding no conclusive proof of a superior thermodynamic stability of racemic crystals. It was eventually proposed[1] that the main reason for the more frequent appearance of crystalline racemates is that in racemic solutions or liquid states the chance of encounter of molecules of opposite handedness is higher than that of pairs of same handedness: thus, not an energy, but a mix of kinetics and entropy reasons. The argument is however highly controversial,[2–5] because many cases of spontaneous resolution do occur.[6–10] Also to be considered is the somewhat disquieting, possible influence of latent chiral impurities, or of heterogeneous crystallization, on which one has no control at all.

In this paper we search for relationships, if any, between complexity in molecular structure (essentially, torsional freedom) and the strength of intermolecular forces on one side, and the relative stability or ease of formation of racemic (*rac*) and homochiral (*hom*) solids on the other side; relationships between the properties of crystalline and liquid systems are also explored. We study first the homochiral or racemic liquid state of a set of small chiral compounds, with or without hydrogen bonding, whose basic core structure is shown in Scheme Ia. Then, we have selected 2-phenoxypropionic acids (PPA's, Scheme Ib) as representative of the *hom*/*rac* equilibria in larger organic compounds. These substances have been studied in a considerable

number because of their agrochemical or pharmacological (analgesic and anti-inflammatory) properties.[11] While *S*-enantiomers of a variety of these acids are the active form of the so-called 'profens' non-steroidal anti-inflammatory drugs (NSAID),[12] the *R*-forms can be employed as herbicides.[13] Besides, they offer a convenient platform for a theoretical study by molecular mechanics or ab initio method, for several reasons: they have only one chiral carbon center, immediately next to the carboxylic group; their molecular structure is complex, and they exhibit conformational flexibility, but calculations by present methods are comfortably manageable; many X-ray crystal structures are available[14] including several pairs of *hom* and *rac* crystals of the same compound. In the final roundup of positive and negative results, some consistent structural effects emerge, but, as may be expected in such a long-standing and debated problem, robust conclusive inferences on the mechanisms of nucleation and chiral separation seem to escape even the most careful analysis by our present arsenal of theoretical methods. Our conclusions are nevertheless valuable in orienting future work in the field, at least by disposing of some preconceived ideas.

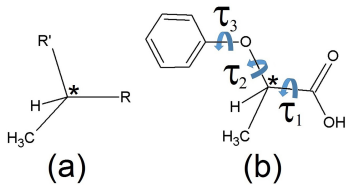

Scheme I. (a) The basic framework around a chiral center (labelled as '*'). (b) 2-phenoxypropionic acids (PPAs), with the three conformation-defining torsion angles.

2. COMPUTATIONAL METHODS

2.1 Crystal and molecular structures and energies. Crystal and molecular structures of PPAs were retrieved from the Cambridge Structural Database[15] (CSD) and are henceforth identified by their CSD refcode (complete information can be found in the Supporting Information, SI: see Tables S1-S4). The usual[16] renormalization of bond distances involving hydrogens was applied (C-H 1.08, O-H 1.00 Å). Some crystals exhibit disorder at the carboxylic group, with C=O and C–O distances nearly identical and undisclosed position for the H-atom. These were reset at $d_{C=O}$ = 1.21, d_{C-O} = 1.31, d_{O-H} = 1.0 Å and angle CÔH = 109°. The configuration at the chiral center is strictly rigid and tetrahedral, and was therefore kept fixed as such in all simulations. The carboxyl group was considered as a rigid planar fragment, and the phenyl rings and their substituents were also modeled as rigid sub-units. For the small molecules (see Scheme II), bond distances and angles were set at standard values obtained from statistics over crystallographic data, and the only degrees of freedom allowed were torsion around the single C–C or C–O bonds. Methyl group libration was routinely allowed. Lattice energies of the PPAs were evaluated by different methods: (i) the atom-atom CLP potential energy scheme,[16] and (ii) the PIXEL method,[17] on the un-deformed crystal structures; (iii) periodic quantum simulations at the DFT B3LYP/6-31G(p,d) level, including relaxation of molecular and crystal structures. All the solid-state DFT calculations have been performed by means of the CRYSTAL09 code.[18] The interested reader can find a full description of the computational quantum mechanical procedure in the Supporting Information (Section S1 SI).

Molecular energies were calculated by DFT or *ab initio* MP2-631G*[19] methods using the molecular structures found in the X-ray crystal structure determinations. Monte Carlo

simulations were carried out in the AA-CLP force field scheme.[16,20] For Z'=1 structures (1 molecule per asymmetric unit), the total crystal lattice energy (E_{latt}) can be defined[21] as the electronic energy of the cell (E_{bulk}) divided by the number of formulae it contains (Z), minus the electronic energy of one molecule keeping its solid-state conformation (E_{mol}). The DFT estimates were also corrected for basis set superposition error,[22,23] E_{BSSE}, and for the molecular relaxation term, E_{rel}, according to (see also Section S1 SI for further details):[24–26]

$$E_{latt} = E_{bulk} / Z - E_{mol} - E_{BSSE} - E_{rel} \quad (1)$$

The conformational analysis of PPAs can be discussed in terms of the three torsion angles (Scheme I), τ_1 (O–C*–C=O), τ_2 (C_{ar}–O–C*–C[COOH]), and τ_3 (C_{ar}=C_{ar}–O–C*). Detailed comments on the derivation of the torsional energy term can be found in the Supporting Information (Section S2). The usual convention for torsion angles is adopted, i.e. the A-B-C-D torsion angle is positive if, looking from A down the B-C bond, the C-D bond is seen turning to the right side. A change of sign of a torsion angle goes with a change in molecular energy, except when the plane defined by the four atoms at $\tau = 0$ is a mirror symmetry plane. For a given molecular configuration, enantiomers have torsion angles of opposite sign without a change in energy. Full details on the physical framework employed to model the torsional degrees of freedom is given in the Supporting Information (Section S2 SI).

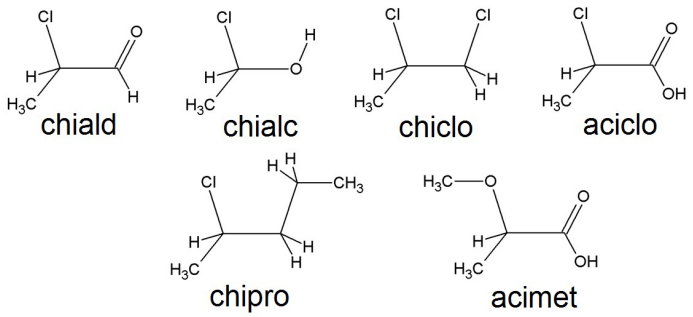

Scheme II. Small chiral molecules for the Monte Carlo simulation of *rac* and *hom* liquids. 2-chloropropionaldehyde (chiald), 2-chloroethanol (chialc), 1,2-dichloropropane (chiclo), 2-chloropropionic acid (aciclo), 2-chloropentane (chipro), and 2-methoxypropionic acid (acimet).

2.2. Monte Carlo simulations. Intermolecular energies in liquids and crystals were calculated in the CLP approximation.[16] Simulations were performed in the semi-rigid approximation, whereby some parts of the molecule are kept at a constant geometry while torsional freedom is allowed between them. The intramolecular force field therefore includes only torsional energy terms. MC runs were carried out using computational boxes of typically 150-200 molecules for crystals and 250 molecules for liquids, with periodic boundary conditions and standard temperature and pressure control.[16,20] Anisotropic starting boxes for the PPA crystals were prepared using multiples of the unit cell. Isotropic computational boxes for the liquids were prepared by constructing a grid of molecules all of one handedness for the *hom* liquid and half of each handedness for the *rac* liquids; starting values of the variable torsion angles were randomized between -180 and +180°. A typical procedure includes 500kstep (1 kstep = 1 thousand MC steps) starting runs without periodic boundaries at 3 K (energy minimization to dispose of hard contacts) followed by gradual warmup to 100 and higher temperatures as required. The last 1-2 Msteps (1 Mstep = 1 million MC steps) of production runs of 10-20 Msteps were used to harvest average energies and structural parameters.

2.3 Reproducibility. All software used in this paper, except for the DFT calculations, has been developed in-house and can be found in source code with complete documentation and worked examples at http://users.unimi.it/gavezzot. All program modules were applied in the standard, long-standing parameterization.[16,17] Complete numerical detail of the input-output files for all simulations can be obtained from the authors upon request.

3. RESULTS AND DISCUSSION

3. 1. Experimental crystal structures

3.1.1. Space groups and conformations. Some relevant crystal data for the PPAs here examined are collected in Table 1. Racemic crystals are in the usual centrosymmetric space groups with an unusually high frequency of *C*2/c. They form a cyclic double hydrogen bond over a center of symmetry. Homochiral crystals have all been obtained from the homochiral solutions, rather than by spontaneous resolution. They are all in space group $P2_1$ and use a catemer type of aggregation with chains of single O-H···O hydrogen bonds. However, this arrangement is far from common: a CSD survey of crystal structures of carboxylic acids in space group $P2_1$ yields only very few cases of catemer formation (besides the crystals already cited in Table 1, see e.g. refcodes COYRUD, DETLEU, FIKJEO, SDPPCX, TETROL01, XONNET, ZZZNQQ). These occur only when there are no other H-bond competitors: when NH groups are present, the carboxyl C=O oxygen acts as acceptor of a N-H···O hydrogen bond; sp^2 nitrogen, ether, alcohol or carbonyl oxygen, when present, invariably act as preferential acceptors of a COH···O or COH···N hydrogen bond with the carboxyl group. One crystal structure, LUNRAN[14i], has space group $P2_12_12$, where a dimer is formed between two independent molecules in the asymmetric unit, related by an approximate twofold axis. The *R*-factor is relatively high (6.9%) so that this could be a metastable polymorph.

Torsion angle τ_2 is in the very narrow 72-86° range. Although the intrinsic barrier for rotation around the C_{ar}-O bond is low (4 kJ mol^{-1}), angle τ_3 is in the 0-17° range, so that the ring and the O–C* vector are almost coplanar. Angle τ_1 is in the 0-33° range for racemic crystals (O–C*–

C=O group in *syn* configuration) and in the 148-178° range for homochiral crystals (O–C*–C=O group in *anti* configuration, see Figure 1).

3.1.2. Static lattice energies. The lattice energies of the static crystal structures of PPAs have been estimated by different methods (Table 2). DFT calculations account just for purely electronic terms (see equation (1): no dispersion and zero-point corrections have been included). In any case, the *rac* crystal is found more stable in all cases by both the approximate atom-atom method and the more accurate DFT simulations, while the PIXEL method predicted the *hom* form as the most stable one just in a couple of cases. Energy differences are always less than 10% of the lattice energies, the same order of magnitude as the differences found in previous analyses[1] and between crystal polymorphs.[27]

Table 1. Crystal structures of phenoxypropionic acids (PPA's). Top or only line of each entry: racemic crystal (*rac*), second line: homochiral crystal (*hom*). See Scheme I for the definition of torsion angles.

phenyl substituents	CSD refcode	space group	torsion angles[a] / °			m.p.[b] /K
			τ_1	τ_2	τ_3	
none	BEFTIP01	*C*2/*c*	24	72	-7	388
	HUSXAU	$P2_1$	-178	77	-1	359
4-chloro	BEFTOV	*C*2/*c*	26	73	-11	-
	FIXQEI	$P2_1$	-152	77	-2	338
2,4-dichloro	IBUHIW	$P\bar{1}$	11	76	-8	-
	IBUHES	$P2_1$	-176	73	-4	395
2-chloro-4-nitro	IBUHUI	$P\bar{1}$	16	75	-5	423
	IBUHOC	$P2_1$	169	84	-15	389
2-bromo	TOHTUG	*C*2/*c*	30	74	-5	383
	TORTEA	$P2_1$	-159	76	-7	370
2,4,5-trichloro	TCPPRA	$P\bar{1}$	16	72	1	-
	LUNRAN	$P2_12_12$, Z'=2[c]	-148,-169	74,78	-10,-10	417
2-methyl-4-chloro	CMPXPA	$P2_1/c$[c]	0	86	17	363

2-chloro	CPHPNC	$P2_1/n$	21	66	1	-
3,5-dichloro	DCPXPA	$P\ \bar{1}$[c]	33	73	3	-
3-chloro	DIRNOH	$C2/c$[c]	29	75	7	386
3,4-dichloro	QIFGUI	$P2_1/c$	16	76	-4	-

[a] Signs of torsion angles are given assuming $\tau_2 > 0$. For *rac* structures, the enantiomer in the same crystal has the same angles with opposite signs, for *hom* structures the molecule in the enantiomer crystal has the same angles with opposite signs.

[b] Experimental melting point, when available from the CSD.

[c] Disorder at the carboxylic group, reset (see text).

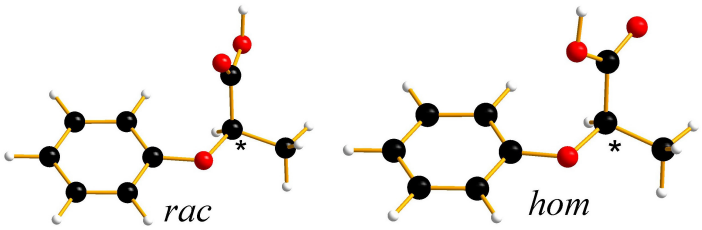

Figure 1. Color online. Conformation-defining torsion angles in PPAs: τ_1, O–C*–C=O; τ_2, C_{ar}–O–C*–COOH; τ_3, C_{ar}=C_{ar}–O–C*, C_{ar} being an aryl carbon. The pictures show a typical conformation in a racemic (BEFTIP) and homochiral (HUSXAU) crystal, with τ_1, which defines the carboxylic acid group, being syn and anti, respectively. Here and in the following molecular schemes, the usual color code is employed for the various atomic species, i.e. oxygen: red; chlorine: light green; bromine: purple; carbon: black; hydrogen: white.

As previously noted,[3] energies calculated on molecules in crystals are highly sensitive to hardly significant structural variations due to small differences in the X-ray determinations. Most important, the experimental uncertainty might introduce significant inaccuracies in the computational results. A crucial point is the well-known difficulty in accurately localizing hydrogen atoms by ordinary X-ray diffraction methods, especially when the experiments are performed at room temperature with standard resolution ($\sin\vartheta/\lambda \leq 0.65$ Å^{-1}). Even small

uncorrected systematic errors influence the estimated thermal parameters, reducing the accuracy of bond distances and, therefore, of hydrogen bond geometries. This obviously could bias the computed HB energies in rather unpredictable ways, resulting in errors that might exceed those due to the intrinsic limitations of the computational method. For example, one may compare the crystal structures of GOGPEY and GOGPIC, *R*- and *S*-phenylpropionic acid, respectively, carried out simultaneously in identical experimental conditions.[28] The two structures should be identical in all respects except for the sign of torsion angles. In fact, the *R*-crystal is 1.5% denser than the *S*-crystal; its Coulombic plus polarization energy is 9.5 kJ mol^{-1} more stabilizing and its total lattice energy is 2.3 kJ mol^{-1} (2.3%) more stabilizing; on the other hand, the MP2/6-31G** molecular energy is lower for *S* by 6.6 kJ mol^{-1}. The origin of these differences can be traced back to a small difference in the C-O-H angle (112° in *R* and 109° in *S*): in the *R*-crystal, the O-H···O hydrogen bond is slightly shorter, more linear and therefore turns out slightly stronger, while the S-molecule is more stable because the CÔH angle is closer to the tetrahedral value. The crystallographic *R*-factor of R is 3.36 against 4.03% for S; however, the position of one hydrogen atom in a 80-electron molecule can hardly have affected the accuracy of the refinement. That position is nevertheless of crucial importance in energy calculations. Thus, random, minor differences in structural determinations are irrelevant to the X-ray crystallographer but may pose a seldom recognized problem to theoretical investigations.

Table 2. Lattice energies and total crystal energies ($kJ \cdot mol^{-1}$) of pairs of *rac* and *hom* PPA's by various computational methods. Intramolecular relaxation terms were taken into account just by DFT simulations (see Section 2.1 above).

	PIXEL partitioned energies	Total lattice energies

rac *hom*	$E_{coul}+E_{pol}$	E_{disp}	E_{rep}	PIXEL[a]	AA	DFT	Total *rac–hom* [b]
BEFTIP01	-135.4	-107.8	136.4	-106.7	-119.6	-27.0	-5.6
HUSXAU	-124.2	-103.6	122.5	+2.5	+4.6	+4.9	
BEFTOV	-134.6	-113.9	125.4	-123.1	-123.1	-27.7	+3.4
FIXQEI	-134.0	-121.9	140.8	+8.1	+5.9	+5.8	
IBUHIW	-127.4	-116.1	123.1	-120.4	-123.9	-30.9	+8.7
IBUHES	-130.7	-125.7	135.8	-0.2	+5.4	+4.1	
IBUHUI	-131.3	-113.0	119.0	-125.3	-136.6	-36.5	+2.1
IBUHOC	-147.4	-128.0	148.6	-1.5	+13.5	+4.5	
TOHTUG	-148.7	-124.7	156.0	-117.5	-125.0	-	-13.8
TORTEA	-111.5	-106.1	105.6	+5.5	+7.6		
TCPPRA	-136.8	-146.4	147.4	-135.9	-127.3	-	-
LUNRAN	-141.0	-142.1	155.0	+7.8	+7.8		

[a] The total lattice energy of the *hom* crystal is given in terms of the difference with respect to the *rac* one.

[b] Difference in lattice energy (PIXEL) + difference in intramolecular energy (not unequivocal for $Z'=2$). Positive values imply that *hom* is the most stable form. Full detail of partitioned energies is found in Tables S3 and S4 SI. Measure units are given in kJ mol^{-1}.

3.1.3. Packing patterns. More revealing than total lattice energies is the analysis of the main structural determinants, that is, the molecule-molecule pairs that are bound by the largest cohesive energies and hence define the basic structural motif in a crystal. Energies are calculated by the PIXEL approach and are subdivided into Coulomb-polarization and dispersion terms, so that they also provide a preliminary understanding of the nature of the chemical potential at work there. Results are shown in Figures 2-3 and in Table 3.

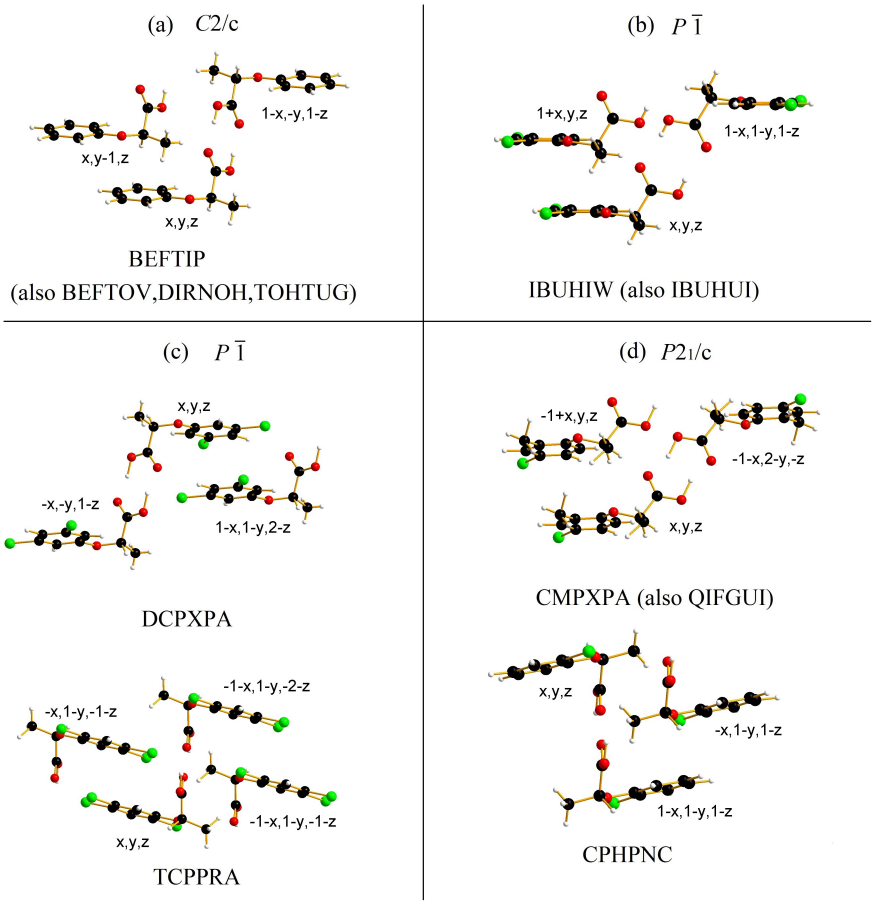

Figure 2. Color online. The main determinants in centrosymmetric crystal structures of *rac* PPAs. See Table 3 for the corresponding interaction energies. Symmetry operations are also highlighted in fractional coordinates. See Fig. 1 for the atom color code.

The *C*2/c structures of the *rac* crystals (Figure 2a) show a cyclic double hydrogen bond over a center of symmetry, with a very strong Coulomb-polarization contribution. Second in importance is a molecular pair with stacked rings and mainly dispersive interactions; the Coulombic contribution is not negligible however, and results from nesting of the positively charged methine and methyl hydrogens into the electron-rich pocket formed by the O–C–C=O bay and the π-cloud of the aromatic ring. Similar packing motifs are adopted by some $P\ \bar{1}$ *rac* crystals (Figure 2b, hereinafter $P\ \bar{1}$ type I motif), but aromatic rings stack at shorter distances and the

interaction is therefore more stabilizing. Other $P\ \bar{1}$ crystal structures (Figure 2c, hereinafter $P\ \bar{1}$ type II motif) are quite different: the contribution of the cyclic double bond is smaller and aromatic ring stacking obtained by centrosymmetric inversion (head-to-tail). Also similar are the motifs in some $P2_1/c$ crystal structures (Figure 2d; compare e.g. CMPXPA and IBUHIW), while CPHPNC is quite different.

The packing motifs in the four isostructural homochiral crystals (HUSXAU, IBUHES, IBUHOC, TORTEA, Figure 3) show a strong interaction between aromatic rings stacked by translation, with a stabilization energy almost always larger than that of the single hydrogen bond in the catemer chain. The FIXQEI crystal adopts a tighter hydrogen-bonded chain, taking advantage also of a contact between the carbonyl oxygen and the region around the acidic methine proton, while aromatic rings are stacked head-to tail along a second screw axis.

Table 3. The main structure determinants in crystal structures of PPAs seen in Figures 2-5. For each pair, symmetry symbol (*i* for inversion, *T* for translation, *S* for screw), center of mass distances (d_{CM}, Å), molecule-molecule energies (kJ·mol^{-1}): Coulombic (E_{coul}), polarization (E_{pol}), dispersion (E_{dis}), repulsion (E_{rep}), total (E_{tot}). See Tables S7-S11 and Figures S2-S5 SI for full details.

Symmetry	d_{CM} / Å	E_{coul}	E_{pol}	E_{dis}	E_{rep}	E_{tot}	Motif
*C*2/c: BEFTIP shown in Fig. 2(a) (BEFTOV, DIRNOH, TOHTUG are very similar, see Supporting Information Fig. S2)							
i	7.281	-130.4	-64.6	-21.1	151.4	-64.7	H-bond dimer
T	5.255	-10.1	-4.9	-25.9	19.2	-21.7	stack
$P\ \bar{1}$: 'Type I' structure determinants: see IBUHIW, IBUHUI in Fig. 2(b)							

i	9.108	-127.2	-65.1	-22.3	145.4	-69.2	H-bond dimer
T	4.472	-13.1	-5.9	-42.5	25.1	-36.4	stack
$P\bar{1}$: 'Type II' structure determinant: see DCPXPA in Fig. 2(c)							
i	8.790	-122.1	-64.2	-23.5	149.5	-60.4	H-bond dimer
i	4.284	-18.1	-6.0	-57.3	37.0	-44.4	stack
$P\bar{1}$: 'Type II' structure determinant: see TCPPRA in Fig. 2(c)							
i	9.033	-122.2	-67.9	-22.6	155.3	-57.5	H-bond dimer
i	7.392	-10.8	-5.5	-33.9	18.7	-31.5	stack
$P2_1/c$ CMPXPA shown in Fig. 2(d)							
i	9.160	-123.9	-65.3	-22.5	148.5	-63.2	H-bond dimer
T	4.395	-9.8	-4.7	-40.6	21.2	-33.9	Stack
$P2_1$: HUSXAU shown in Fig. 3(a) (IBUHES, IBUHOC are very similar, see Supporting Information Fig. S5)							
T	4.832	-19.0	-5.1	-29.0	22.5	-30.6	stack
S	7.929	-51.6	-27.9	-11.4	67.7	-23.2	H-bond catemer
$P2_1$: FIXQEI shown in Fig. 3(b)							
S	8.203	-70.2	-35.0	-16.5	83.5	-38.2	H-bond catemer
S	4.951	-4.4	-4.0	-34.1	21.0	-21.5	stack
$P2_12_12$: LUNRAN shown in Fig. 4(a-b)							
asymm.	7.526	-131.9	-75.5	-26.4	171.1	-62.8	approx. twofold

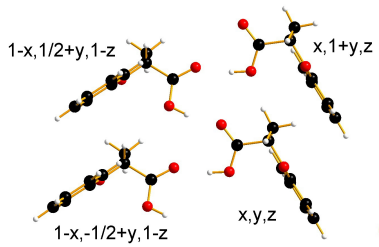

(a)

HUSXAU (also IBUHES, IBUHOC, TORTEA)

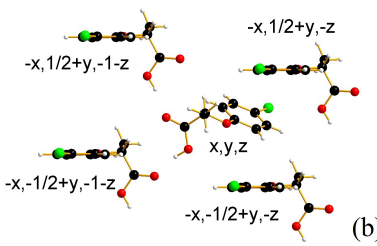

(b)

FIXQEI

Figure 3. Color online. The dominating packing motifs in the $P2_1$ crystal structures of PPAs. (a) HUSXAU, (b) FIXQEI. See Table 3 for the interaction energies and Fig. 1 for the atom color code.

Figure 4 shows a cyclic dimer formed by two symmetry-independent molecules related by a *pseudo*-twofold axis. The PIXEL analysis (Table 3) suggests that the hydrogen bond is even stronger than in the centrosymmetric case, and that the dimer is stabilized by a slightly higher dispersive contribution, presumably arising from proximity of the highly polarizable chlorine atoms. Why is then that the twofold axis, in general, is never adopted in real crystal structures? The distribution of electron density in the object in Figure 4a-b makes it more difficult to pack into a three-dimensional structure than the centrosymmetric dimer. Transforming this qualitative view into some quantitative indicator is a very challenging task, as finding a quantitative descriptor of the packing adaptability of a given molecular object would be a major step forward in our understanding of molecular crystals.

Figure 5 shows at a glance the overall energetic landscape of the PPA crystal structures. Both *hom* and *rac* structures are mainly stabilized by hydrogen bonding and aromatic ring stacking, although the energetic value of these two effects may vary by as much as 30% for compounds of very similar chemical composition, depending on minor modulations of the molecular structure. Two single O···H hydrogen bonds of the catemer structure are less stabilizing ($E < 60$ kJ·mol^{-1}) than the cyclic double hydrogen bond ($E > 60$ kJ mol^{-1}).

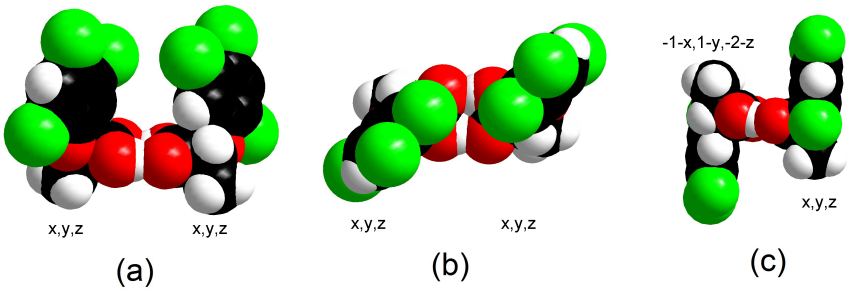

Figure 4. (a) and (b): Two space-filling views of the nearly twofold-symmetric dimer in the crystal structure of LUNRAN; (c) the centrosymmetric dimer in the corresponding *rac* crystal TCPPRA.

Stacking along the screw axis that supports the catemer chain may be equivalent or even more stabilizing than the single hydrogen bond itself, challenging the common wisdom that H-bonding is always the first strongest interaction in crystals. Pair energies other than closest-neighbor ones merge in a sort of continuum decreasing with increasing distance. Relative overall stabilities may then be dictated by first-neighbour arrangement or may be subtly modulated by long-range interactions. One sees a wide choice of packing arrangements, which, as is so often the case in studies of packing patterns, cannot be rationalized by chemical intuition: for example, the unsubstituted compound is isostructural with the 3-chloro, 4-chloro and 2-bromo compounds, but not with 2-chloro or 3,5-dichloro. The 2-chloro-4-nitro compound, whose nitro functionality introduces a distinct electronic request, is almost isostructural with the more mildly substituted 2,4-dichloro compound.

Figure 5 also shows two patent outliers in their centre-of-mass distance, whose structure is shown in Figure 6: for these relatively strong interactions there is no clear-cut description in structural terms, warning against judging crystal structures only in terms of popular, standard

concepts. Even less convincing may be analyses of relative stabilities by misleading oversimplifications like C-H···O, C-H···π, halogen bonding, and the like. [29]

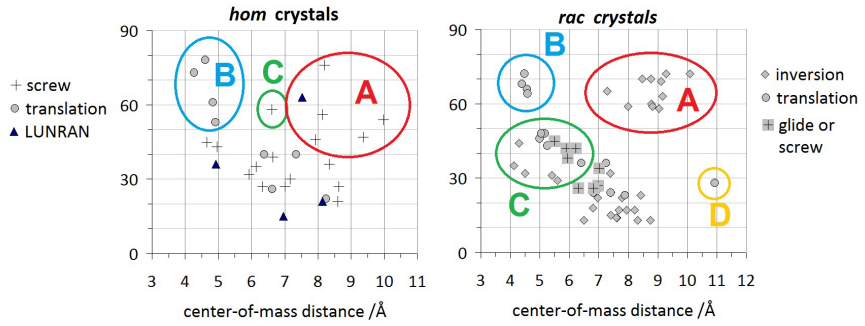

Figure 5. Color online. Plots of the molecule-molecule interaction energies in PPA crystals. *hom* crystals, left: A, hydrogen-bonded chain structures along screw axes and cyclic asymmetric dimer in LUNRAN; B, corresponding translations; C, IBUHOC, see Figure 6. *rac* structures, right: A, cyclic dimers over centers of symmetry, coupled with B, tight stacking in $P\ \overline{1}$ or $P2_1/c$ structures, or C, looser stacking and glide-related pairs in $C2/c$ structures. D: IBUHUI, see Figure 6. In datasets for screw axes and translations, molecule-molecule energies are doubled since each molecule interacts with two identical partners.

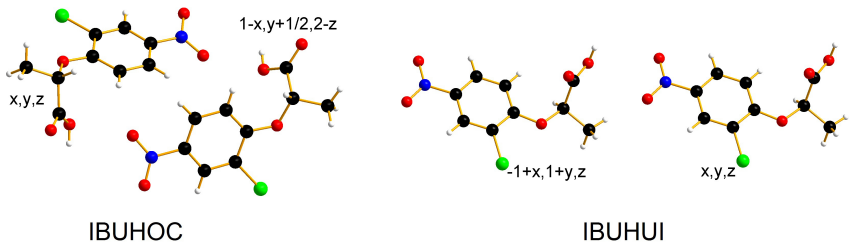

Figure 6. Very stabilizing molecule-molecule pairs, as identified in Figure 5. Both involve a number of diffuse, hardly classifiable contacts ranging from nitro-carboxyl interactions to nitro oxygen-acidic hydrogen interactions.

3.2. syn or anti O–C*–C=O? The O–C*–C=O group is systematically *anti* (τ_1 close to 180°) in *hom* crystals and *syn* (τ_1 close to 0°) in *rac* crystals (Table 1). For chiral crystal structures a plausible explanation is that a *syn* configuration at the O–C*–C=O bay would cause unfavorable O···O contacts between translation-related pairs along the screw axis (Figure 7). The case with *rac* crystals and their wider choice of packing patterns is not clear-cut. The CSD was searched for O–H···O=C hydrogen bonds in the fragment R–O–C–C=O. Of the 59 centrosymmetric cyclic hydrogen bonds so found, 63% have $0°<\tau_1<10°$, 75% $0°<\tau_1<20°$, and 94% $0°<\tau_1<40°$. This result confirms that the *syn* arrangement is independent of space group and of chemical environment, and is therefore due to a relative stability either of the monomers or of the dimers. Molecular energies were calculated at the MP2/6-31G** level for two small molecules, ACIMET (Scheme 2), and ACI, in which the methyl group is replaced by a hydrogen atom to avoid steric interference: *anti*-ACIMET is more stable by 4.7 kJ mol^{-1}, and *anti*-ACI by 2.5 kJ mol^{-1}. Since these energies were calculated without molecular relaxation, the differences are upper estimates, and may well be insignificant in real life.

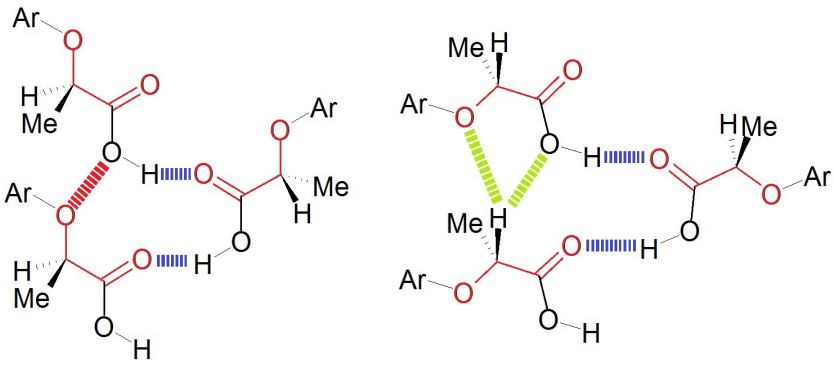

Figure 7. Color online. Screw chains in $P2_1$ homochiral crystal structures. Left: unfavorable oxygen-oxygen contacts (red, dashed) between translation-related molecules O–C–C=O *syn* configuration (not adopted). Right: proximity of the acidic (aliphatic C-H) part of the molecule

to the electron-rich cavity (light green, dashed) when O–C–C=O is in the *anti* configuration. Possible strong hydrogen bonds are marked in blue.

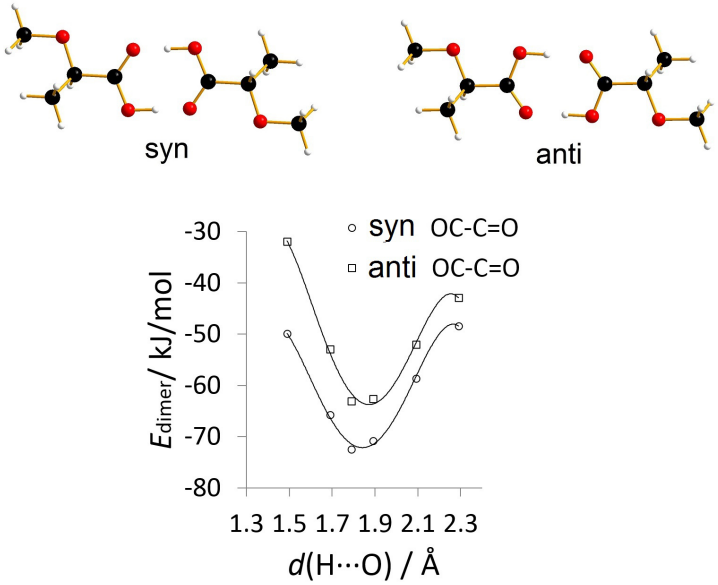

Figure 8. Top: dimers with carboxyl group in *anti* and *syn* configuration. The difference is mainly due to C-C-O and C-C=O angles (114 and 122°, respectively). Bottom: dimerization energies. The minima are at the same distance but the *anti* dimers are ≈ 10 kJ·mol^{-1} less stable than the *syn* ones.

PIXEL dimer calculations were performed for the formation of the centrosymmetric dimers in the *syn* and *anti* configurations: Figure 8 shows the considerable structural difference between the two cases. The dimerization energy is more favorable by 10 kJ mol^{-1} for the dimer in *syn* configuration. Therefore, the *syn* configuration is not a crystal packing effect, but must be picked up at dimer formation time and preserved at crystallization stage.

3.2. Monte Carlo simulations.

3.2.1. Validation of the atom-atom force field. As a check of the reliability of the force field we have carried out 10Mstep Monte Carlo runs on the crystal structures of four couples of *rac-hom*

PPAs. The temperature was set at 350 K, close to the melting temperatures of all the compounds (Table 1). Results are shown in Table 4. For energies, the simulations correctly show the expected destabilization with increasing temperatures due to increase in intramolecular energies and decrease in cohesive energies. For densities, the results are mostly reasonable, with a few exceptions. Cell parameter changes are very small (Table S12 SI).

A further confirmation of the reliability of the force field comes from a plot of calculated enthalpies of vaporization *vs.* enthalpies of sublimation, in comparison with a set of experimental data for general organic compounds. Calculated values were estimated from the cohesive energies of liquids and crystals (E_{dis}+E_{rep}+E_{pol}+E_{coul}), neglecting the small differences in intramolecular energies.[30] Figure 9 shows that our calculated values are well within the expected range.

Table 4. Monte Carlo simulations on PPA crystals with the AA-CLP force field.[a] For each entry, top line, starting point (experimental crystal structure); second line, variation from the low-T crystal structure after a 10 Mstep MC run. Measure units are expressed as kJ·mol^{-1}.

	Density / g·cm^{-3}	T/ K	*E*(intramol.)	E_{LP} [b]	E_{coul}	E_{tot}
BEFTIP *rac*	1.35	122	3.3	-79.7	-36.1	-112.6
	-0.03	350	+0.4	+2.2	+5.1	+7.8
HUSXAU *hom*	1.32	122	5.7	-78.0	-33.1	-105.5
	-0.02	350	+1.5	+2.7	+5.3	+9.5
BEFTOV *rac*	1.42	298	2.7	-83.5	-36.2	-117.0
	+0.01	350	+0.5	-0.7	+6.2	+6.1
FIXQEI *hom*	1.47	122	3.8	-86.0	-28.1	-110.3
	-0.01	350	+0.2	0.0	+5.9	+6.1
IBUHIW *rac*	1.49	298	3.0	-85.5	-35.4	-117.9

	+0.06	350	+0.6	-4.7	+4.2	+0.2
IBUHES *hom*	1.53	153	5.4	-86.7	-28.6	-109.9
	0.0	350	+1.9	+0.7	+3.7	+6.3
IBUHUI *rac*	1.53	298	3.1	-90.8	-39.2	-127.0
	+0.01	350	+0.5	+3.0	+5.3	+1.7
IBUHOC *hom*	1.59	153	6.6	-87.8	-29.1	-111.2
	-0.07	350	+2.6	-5.1	+6.3	+4.6

[a] See also Figure 9. Computed sublimation enthalpies, when compared with the corresponding vaporization enthalpies of simulated liquids, correlate well with experimental estimates, as a further proof of the reliability of the AA-CLP force field.

[b]In the Coulomb-London-Pauli (CLP) model,[16] E_{LP} includes dispersion, polarization and repulsion terms.

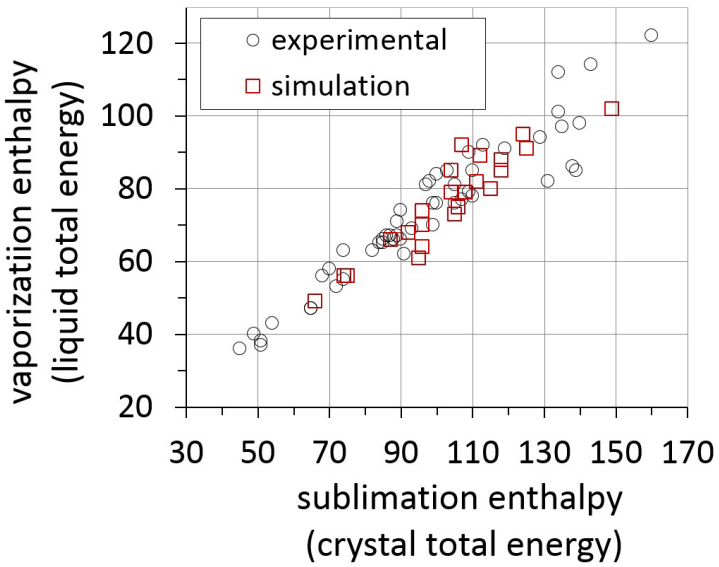

Figure 9. Vaporization *vs.* sublimation enthalpies: calculated data (red squares) and experimental data (black circles) are for a variety of organic compounds.[31] All quantities are given in kJ·mol^{-1}. See Supporting Information (Table S13 and Figure S6 SI) for more details.

3.2.2 Liquid state of model compounds. In search of differences between homochiral and racemic systems other than in crystals, we have simulated the liquid state of some model chiral compounds (Scheme 2): They differ in molecular size, in flexibility, and in the physical nature of the intermolecular interaction. Results are shown in Table 5. Agreement with experiment is very good. The trends in correlation functions are as expected: weakly bound liquids show higher diffusivity and quicker decay of rotational correlation. Translational correlation seems to indicate a lower diffusivity (higher viscosity) of *hom* liquids; this results is at the borderline of significance but is systematic. We have no straightforward interpretation for it.

Energies and densities of *hom* and *rac* liquids are identical within computational accuracy. Neither hydrogen bonding nor the presence of flexible or dangling groups seem to induce a significant difference in stability between these homochiral and racemic liquid phases.

3.2.3. PPA liquids. A common molecular structure for each pair of *rac* and *hom* systems was prepared as a starting point using an average of the bond distances, bond angles and fixed torsion angles found in the crystal structures - differences are always very small. Table 6 shows the results of the MC simulations in terms of energy contributions and densities. The agreement with the scarce experimental data available ranges from acceptable to excellent.

Table 5. Calculated properties of the racemic and homochiral liquid phases of some test compounds (see scheme II) at 300 K.

	E_{intra}	E_{LP}	E_{Coul}	E_{tot}[a]	density[b] / g cm^{-3}	density, exp	ΔH_{vap}, exp calc[c]	corr. functs tras rot[d]
chiald *rac*	3.6	-24.8	-19.9	-41.0	1.117	-	- -	2.17 0.67

hom[e]	+0.2	+0.2	-0.1	+0.2	1.111	-	- -	2.09 0.67
chialc *rac*	3.1	-32.7	-24.8	-54.3	1.211	-	- -	1.37 0.85
hom	-0.1	-0.3	+0.2	-0.3	1.216	-	- -	1.12 0.88
chiclo *rac*	4.6	-27.9	-2.8	-26.0	1.141	1.156	34-39 32	4.55 0.46
hom	0.0	-0.4	0.0	-0.5	1.155	-	- -	3.99 0.47
aciclo *rac*	2.7	-37.5	-19.7	-54.6	1.276	1.18	63-65 59	1.53 0.88
hom	-0.2	-0.3	-0.2	-0.5	1.286	-	- -	1.03 0.91
chipro *rac*	8.1	-32.0	-0.8	-24.7	0.868	0.87	32-36 33	3.49 0.69
hom	+0.4	0.0	0.0	+0.4	0.866	-	- -	3.25 0.66
acimet *rac*	8.4	-41.3	-26.1	-59.0	1.092	-	- -	0.96 0.93
hom	+0.2	+0.3	+0.6	+1.1	1.084	-	- -	0.92 0.93

[a] Standard deviation of the average 0.3-0.5 kJ mol^{-1}.

[b] Standard deviation of the average 0.006 to 0.011 g cm^{-3}.

[c] Experimental energies are from htttp://nist.webbook.

[d] Center-of-mass translational mean free path and central bond rotational correlation function at the end of a 2Mstep equilibrium run.

[e] A positive difference indicates less stability.

The energies and densities of *rac* and *hom* liquids of the PPAs are identical within the expected accuracies. This result is consistent with that obtained for smaller molecules. The smaller enthalpies of fusion for the *hom* crystals merely reflect the difference in stability between the crystalline states. We find however a significant difference between molecular conformations: in the liquid (Figure 10) the C=C–O–C* angle τ_3 is much larger than in the solid, keeping the bulky substituent groups more clear of contact with the H or Cl atoms flanking the C-O exocyclic bond, and giving the molecule an overall more elongated shape. As expected, the

orientation of the COOH group (τ_1) is almost free in the liquid, with a minor preferences for the *syn* configuration (τ_1=0°). The data for intramolecular energy in liquids and crystals (Tables 5 and 6) show that the cost of these conformational differences (at least according to our force field) is very small, of the order of 2-3 kJ·mol^{-1}.

Table 6. Equilibrium energies (kJ·mol^{-1}) in the Monte Carlo simulation of racemic and homochiral PPA liquids at 350 K. Averages over the last 1 Mstep of equilibrium simulation.

substituent(s) at ring		E_{intra}	E_{LP}	E_{Coul}	E_{tot}[a]	density[b] /g·cm^3	ΔH_{fus}[c] calc	exp[d]
none	*rac*	6.8	-62.6	-18.6	-74.3	1.143	31	33
	hom	-0.2	+0.3	-0.5	-0.4	1.137	21	23
4-chloro	*rac*	4.8	-69.0	-18.4	-82.6	1.265	28	38
	hom	+1.6	+0.7	+0.1	+2.4	1.253	24	23
2,4-dichloro	*rac*	6.2	-75.1	-17.1	-86.0	1.381	31	-
	hom	-0.2	-0.3	+0.3	-0.1	1.388	18	-
2-chloro-4-nitro		7.8	-76.9	-23.2	-92.3	1.359	33	-
		-0.4	-0.7	-0.7	-1.7	1.359	14	-

[a] Standard deviation of the average 0.4-0.7 kJ mol^{-1}.

[b] Standard deviation of the average 0.005 to 0.009 g cm^{-3}.

[c] Enthalpies of fusion are the difference between total energies of the liquid and of the solid (Table 4).

[d] See Ref. 32.

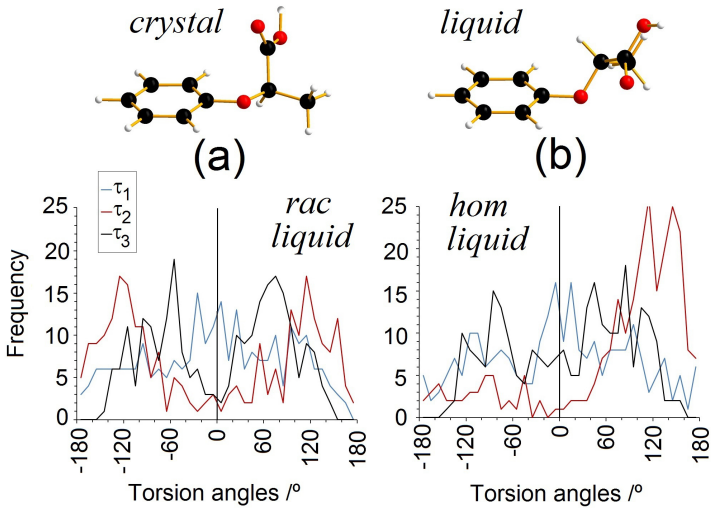

Figure 10. Color online. Top: crystal conformation (a) and liquid conformation using average liquid-state torsion angles (b). Bottom: distribution of torsion angles in the liquid of *rac* (left) and hom (right) 2,4-dichloroPPa at 350 K, as representative of all other compounds. τ_1 and τ_2 peaks spread around 120°, and τ_3 peaks around 70°, while in the crystal the corresponding values are 23, 72 and 7° respectively. The signs have an absolute meaning only for the *hom* liquid because the *rac* liquid contains isomers with torsion angles of opposite sign.

3.2.4. Hydrogen bonding in liquids. Figure 11 shows the evolution of O-H···O=C hydrogen bonding during the stationary state of the liquid simulations of the PPAs. Considering the temperature of 350 K, a contact is defined as a hydrogen bond if the O···H distance is less than 2.2 Å, but results are qualitatively similar using shorter thresholds.

An average 44% of the molecules are engaged in hydrogen bonding involving the acid group when the nitro group is not present, but only 32% do so in nitro derivatives, where nitro oxygen competes as a hydrogen bond acceptor. The number of cyclic double bonds is indeed stable and

identical in *rac* and *hom* liquids, as well as in liquids of different compounds. The number of single hydrogen bonds oscillates more widely, without a clear trend with respect to handedness.

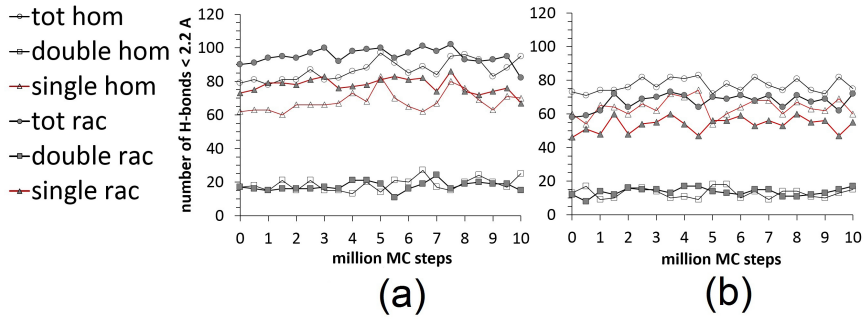

Figure 11. Color online. Number of O-H···O=C hydrogen bonds (O···H distance < 2.2 Å), single, double (cyclic) and total in the liquids of PPAs: (a) 2,4-dichloro, (b) 2-chloro-4-nitro derivatives. Results for the other two pairs (Figure S7 SI) are qualitatively very similar to (a).

4. CONCLUSIONS

A computational study of pairs of *rac-hom* crystal structures of carboxylic acids reveals that *rac* structures are often more stable than *hom* structures, but not exclusively, with many exceptions to what is sometimes considered an established rule (Wallach's rule[2]). This result is in line with previous studies on an ever wider range of chemical classes, including zwitterionic aminoacids.[1,3] A more in-depth analysis of packing modes, using molecule-molecule pairing energies calculated by PIXEL with subdivision into Coulombic-polarization and dispersion terms, shows a competition between the two, with dispersion sometimes compensating or overcompensating for differences in Coulombic energies; in fact, dispersion-related stacked pairs are often more energetic that hydrogen-bonded pairs in homochiral crystals.

Assessing the nature and effects of differences between *rac* and *hom* crystals is not an easy task. They are after all made by the same molecule and may make use of the same intermolecular

attachment points. Considering the landscapes shown in Figures 2, 3 and 5, one is led to the conclusion that flexible and multi-functional organic molecules can always find ways of reaching more or less the same stability irrespective of the availability of certain symmetry operators. Inversion centers are traditionally considered to be more efficient items from the point of view of close packing, but when the complete picture of physical interactions is taken into account, this space-based, old-time concept loses much of its appeal. In simpler words, homochiral systems do not appear to be more "difficult" to pack into a crystal than racemic systems.

What is for sure is that calculated energy differences between *rac* and *hom* crystals are always very small, and it may be thought that an improvement in accuracy of the calculations might change the picture. Accounting for temperature differences, or including differences in entropy or zero-point energy, are other sources of concern, all such terms being of the same (small) order of magnitude and fraught with a number of computational uncertainties. For these reasons, such improvements are not easy to achieve; also, besides the deficiencies in theory, because of random variance of minor structural features, in particular the exact position of hydrogen atoms (ill-defined in X-ray diffraction studies) especially in a hydrogen bond, where small geometry changes imply energy changes of several kJ mol^{-1}. For this reason we draw our conclusion, the substantial similarity between *rac* and *hom* crystal packing, rather from comparisons of the type and distribution of the main determinants of the crystal structure rather than from comparisons of total lattice energies. Incidentally, we may point out that our semiempirical methods are validated by a number of results obtained in this work: for the atom-atom version, by Figure 9, for example; and the PIXEL energy breakdown has been shown to be very nearly as accurate as first principle SAPT calculations.[33]

We do not trust arguments based on crystal density differences, which show an even higher dispersion than differences in energy, with the added difficulty that due to quite a number of minor technical details, density differences between X-ray studies of the same crystal may well be of the same order of magnitude than typical differences between *rac* and *hom* structures. The case is similar to that of crystal polymorphs, where establishing the 'stable' phase at a given temperature is a hard task. In fact, *rac-hom* dualism may be viewed as a peculiar form of polymorphism.

In an attempt to track the origin of supposed different stabilities, we have studied and compared the equilibrium properties of homochiral and racemic liquids. Again, our methods were unable to reveal any difference in thermodynamic properties or in internal structure; same energy and density, same distribution of key contacts. Intuitively, this is a reasonable result, given the higher temperature of the liquid and its translational and diffusional freedom, which may well smear out any bias (if there be) due to the nature and directionality of the intermolecular interaction. Coupling these crystal- and liquid-state results, we come to the tentative conclusion that there is very little chance of identifying, let alone separating, homochiral from racemic phases in absence of X-ray diffraction or of some kind of chiral probe, unless of course one is able to obtain the complete phase diagram by the thermodynamics of mixing - also not a trivial task.

Why then is racemic crystallization more frequent than spontaneous homochiral separation? Consider a liquid made of an equal number of *R* and *S* molecules. The very first chances of encounter and pairing are 50-50, but as soon as, say, an *R-R* aggregation occurs, the number of free *R* molecules around this primitive pair decreases, so that the chances of further aggregation of other partners for homochiral nucleation decrease exponentially with increasing number of

aggregate molecules. And even supposing that homochiral aggregation be much stronger than racemization (which, as we have demonstrated, is unlikely in terms of cohesive energy), there must be a considerable time lag before heat and mass transport may restore a kinetically competitive number of homochiral addends, a time in which molecules of opposite handedness have plenty of chances of getting in the way. At the other extreme, *R*-*S* nuclei can always find a steady number of partners for further aggregation. In this perhaps oversimplified picture we see a case in which thermodynamics will never be able to defeat kinetics. Note that this discussion applies equally well to pure liquids and to solutions, where the first step in aggregation is increasingly believed to imply the formation of liquid droplets.[34] An evolutionary trace of this nucleation struggle may be the fact the *hom* crystals grown from pure *hom* liquids are sometimes of better quality than *rac* crystals out of *rac* liquids. A less palatable hypothesis (hardly demonstrable but also not easily dismissible) on conglomerate formation is that such cases may result from unintentional homogeneous or worse, heterogeneous seeding.

We show that the comparison of crystal and liquid simulations provide reliable information on the conformational changes that occur when flexible molecules pack into the crystal. For example, while the orientation of carboxyl groups in the liquid is random, with free rotation about the C-COOH bond, when there is an oxygen atom at the β-position (in an O-C-COOH fragment) the O-C-C=O torsion angle is preferentially close to zero when cyclic H-bonded dimers are formed; this appears from a survey of existing structures, and our calculation of dimerization energies show a clear advantage for that arrangement. Also, the overall shape of the phenoxypropionic acid molecules changes dramatically from the prevailing configuration adopted in the liquid state, due to packing requirements. This information, if difficult to interpret, is indispensable for in-depth analysis. In this respect, the study of crystal formation and stability

cannot rely on global descriptors or on total energies of the involved phases - even less on qualitative geometric concepts like localized intermolecular distances or patterns of supposed weak interactions. Significant progress in obtaining the crucial information on relative stabilities can only come from high-quality molecular dynamics or Monte Carlo simulations of the transitions. That is where the future lays in crystal structure prediction and control, in such hot fields as polymorph chemistry, cocrystals formation, or chiral separation.[35]

REFERENCES

1 Gavezzotti, A.; Rizzato, S. *J. Org. Chem*. **2014**, *79*(11), 4809–4816.

2 Pratt Brock, C.; Schweizer, W. B.; Dunitz, J. D. J. *Am. Chem. Soc*., **1991**, *113*(26), 9811–9820.

3 Dunitz, J. D.; Gavezzotti, A. J. *Phys. Chem. B* **2012**, *116*, 6740–6750.

4 Fasel, R.; Parschau, M.; Ernst, K.–H. *Nature* **2006**, *439*(7075), 449–452.

5 Li, Z. J.; Ojala, W. K.; Grant, D. J. W. *J. Pharm. Sci.* **2001**, *90*, 1523–1539.

6 Hendi, M.S.; Davis, R.E.; Wheeler, K.A. *Cryst. Eng*. **2000**, *3*, 209–224.

7 Lahav, M.; Leiserowitz, L. *Angew. Chem. Int.Ed.* **1999**, *38*, 2533–2536.

8 Norsten, T.B.; McDonald, R.; Branda, N.R. *Chem. Commun*. **1999**, *8*, 719–720.

9 Pallavicini, M.; Bolchi, C.; Di Pumpo, R.; Fumagalli, L.; Moroni, B.; Valoti, E.; Demartin, F. *Tetrahedron: Asymm*. **2004**, *15,* 1659–1665.

10 D'Oria, E.; Karamertzanis, P.G.; Price, S.L. *Cryst. Growth Des*. **2010**, *10*, 1749–1756.

11 Azzolina, O.; Collina, S.; Vercesi, D.; Ghislandi, V.; Bonabello, A.; Galmozzi, M. R., *Il Farmaco* **1997**, *52*(6-7), 449–456,

12 Rainsford, K. D. *Ibuprofen. A critical bibliographic review*, **1999**, Taylor & Francis, London (UK) ISBN 978-0748406944.

13 Viswanathan, B.; Sivasanker, S.; Ramaswamy, A.V. *Catalysis: principles and applications*, **2002**, Narosa Publishing House, New Delhi (IN) ISBN 81-7319-375-4

14 (a) BEFTIP01, HUSXAU: Sørensen, H. O.; Larsen, S. *Acta Crystallogr*. **2003**, *B59*, 132–140. (b) BEFTOV: Kennard, C. H. L.; Smith, G.; White, A. H. *Acta Crystallogr*. **1982**, *B38*, 868–875. (c) FIXQEI: Sørensen, H. O.; Collet, A; Larsen, S. *Acta Crystallogr*. **1999**, *C55*, 953–956. (d) CMPXPA: Smith, G.; Kennard, C. H. L.; White, A. H.; Hodgson, P. G. *Acta Crystallogr*. **1980**, *B36*, 992–994. (e) CPHPNC: Smith, G.; Kennard, C. H. L.; White, A. H. *Acta Crystallogr*. **1981**, *B37*, 275–277. (f) DCPXPA: Smith, G.; Kennard, C. H. L.; White, A. H. *Acta Crystallogr*. **1978**, *B34*, 2885–2887. (g) DIRNOH: Mak, T. C. W.; Smith, G.; Kennard, C. H. L. *Acta Crystallogr*., **1986**, *C42*, 310–312 (h) INUHES, IBUHIW, IBUHOC, IBUHUI: Hendi, M. S.; Davis, R. E.; Lynch, V. M.; Wheeler, K. A. *Crystal Engineering* **2001**, *4*, 11–24; (i) LUNRAN: Fomulu, S.; Hendi, M. S.; Davis, R. E.; Wheeler, K. A. *Cryst. Growth & Des*. **2002**, *2,* 637–644; (j) QIFGUI: Akhtar, T.; Rauf, M. K.; Ebihara, M.; Hameed, S. *Acta Crystallogr*. **2007**, *E63*, o2590–o2592; (k) TCPPRA: Smith, G.; Kennard, C. H. L.; White, A. H.; Hodgson, P. G. *Acta Crystallogr*. **1977**, *B33*, 2922–2924; (l) TOHTUG, TORTEA: Breen, M. E.; Tameze, S. L.; Dougherty, W. G.; Kassel,W. S.; Wheeler, K. A. *Cryst. Growth & Des*. **2008**, *8*, 3863–3870.

15 Allen, H. *Acta Cryst.*, **2002**. *B58*, 380–388.

16 Gavezzotti, A. *New J. Chem*. **2011**, *35*, 1360–1368.

17 Gavezzotti, A. *Mol. Phys.* **2008**, *106*, 1473-1485..

18 Dovesi, R.; Saunders, V. R.; Roetti, C.; Orlando, R.; Zicovich-Wilson, C. M.; Pascale, F.; Civalleri, B.: Doll, K.; Harrison, N. M.; Bush, I. J.; D'Arco P.; Llunell, *M. CRYSTAL09 User's Manual*, **2009**, University of Torino, Torino, Italy.

19 Frisch, M. J.; Trucks, G. W.; Schlegel, H. B.; Scuseria, G. E.; Robb, M. A.; Cheeseman, J. R.; Scalmani, G.; Barone, V. et al. *Gaussian 09, Revision D.01* Gaussian, Inc., **2009**, Wallingford CT, USA

20 Gavezzotti, A.; *New J. Chem.* **2013**, *37*, 2110–2119.

21 Civalleri, B.; Doll, K.; Zicovich–Wilson, C. M. *J. Phys. Chem. B* **2007**, *111*, 26–33.

22 Boys, S. F.; Bernardi, F. *Molecular Physics* **1970**, *19*, 553-566.

23 The counterpoise method was employed throughout to achieve the BSSE correction. All the ghost atoms within 7.0 Å from the reference molecule were taken into account.

24 Lo Presti, L.; Sist, M.; Loconte, L.; Pinto, A.; Tamborini, L.; Gatti, C. *Crystal Growth & Des*. **2014**, *14*, 5822–5833.

25 Lo Presti, L.; Soave, R.; Longhi, M.; Ortoleva, E. *Acta Crystallogr*. **2010**, *B66*, 527–543.

26 Lo Presti, L.; Ellern, A.; Destro, R.; Lunelli, B. *J. Phys. Chem. A* **2009**, *113*, 3186–3196.

27 Cruz–Cabeza, A. J.; Bernstein, *J. Chem. Rev*. **2014**, *114*(4), 2170–2191.

28 Lemmerer, A.; Bathori, N. B.; Bourne, S. A.; *Acta Cryst*. **2008**, *B64*, 780–790.

29 Thakur, T. S.; Dubey R.; Desiraju, G. R. *IUCrJ* **2015**, *2*, 159–160.

30 Sample simulations of the gas phase using a liquid-like box with 250 molecules located at a distance of about 100 Å and given only intramolecular degrees of freedom yield the sensible result that all average intramolecular energies are 4±1 kJ mol^{-1} at 350 K.

31 Acree, W. and Chickos, J. S. *J. Phys. Chem. Ref. Data* **2010**, *39*, 1–942.

32 Gabard, J.; Collet, A. *Nouveau J. Chim*. **1986**, *10*, 685–690.

33 Moggach, S.A.; Marshall, W.G.; Rogers, D.M.; Parsons, S. *CrystEngComm* **2015**, *in press*

34 Myerson, A. S.; Trout, B. L. *Science* **2013**, *341*, 855–856.

35 Giberti, F.; Salvalaglio, M.; Parrinello, M. *IUCrJ* **2015**, *2*, 256-266.

Insert Table of Contents Graphic and Synopsis Here

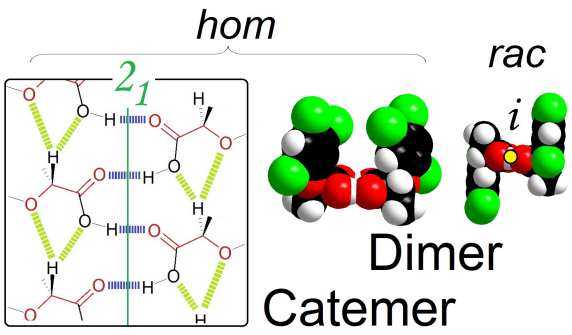

Synopsis: Cyclic hydrogen bonded structures are predominantly associated to racemates, while catemer motifs prevail in homochiral phases. A modeling study of racemic and homochiral liquid and crystalline carboxylic acids reveals and quantifies these and other preferences, but confirms that the distinction between these states, and the propensity for spontaneous resolution, are elusive and may depend on kinetic rather than thermodynamic factors.